CO_2 stripping from ionic liquid at elevated pressures in gas-liquid membrane contactor

Bazhenov, Stepan; Malakhov, Alexander; Bakhtin, Danila; Khotimskiy, Valery; Bondarenko, Galina; Volkov, Vladimir; Ramdin, Mahinder; Vlugt, Thijs J.H.; Volkov, Alexey

DOI
10.1016/j.ijggc.2018.03.001

Publication date
2018

Document Version
Accepted author manuscript

Published in
International Journal of Greenhouse Gas Control

CO_2 stripping from ionic liquid at elevated pressures in gas-liquid membrane contactor

Stepan Bazhenov[1*], Alexander Malakhov[1], Danila Bakhtin[1], Valery Khotimskiy[1], Galina Bondarenko[1], Vladimir Volkov[1], Mahinder Ramdin[2], Thijs J.H.Vlugt[2], Alexey Volkov[1]

[1]A.V.Topchiev Institute of Petrochemical Synthesis RAS, Leninsky prospect 29, 119991, Moscow, Russian Federation

[2]Process & Energy Department, Delft University of Technology, Leeghwaterstraat 39, 2628CB, Delft, the Netherlands

[*] Corresponding author. Tel.: +7 (495) 955-48-93; Fax: +7 (495) 633-85-20; E-mail: sbazhenov@ips.ac.ru.

Abstract

In this study, the gas-liquid membrane contactor was considered for regeneration of the room-temperature ionic liquids (RTIL) that can be used as physical solvents for carbon dioxide capture process at elevated pressures. Poly[1-(trimethylsilyl)-1-propyne] (PTMSP) was selected as a membrane material due to its high mass transport characteristics and good mechanical properties. Nine different RTILs, such as [Emim][DCA], [Emim][BF_4], [Emim][DEP], [Bmim][BF_4], [Bmim][Tf_2N], [Hmim][TCB], [P66614][DCA], [P66614][Br] and [P66614][Phos], were used to evaluate the solvent-membrane compatibility. The long-term sorption tests (40+ days) revealed that the solvent-membrane interaction is mainly determined by the liquid surface tension regardless of viscosity and molecular size of RTILs. For instance, [Emim][BF_4] and [Emim][DCA], having the surface tension of 60.3 and 54.0 mN/m, demonstrated a very low affinity to the bulk material of PTMSP (sorption as low as 0.02 g/g; no swelling); while for the next ionic liquid [Bmim][BF_4] with surface tension of 44.4 mN/m, the sorption and swelling of PTMSP was 0.79 g/g and 21%, respectively. The long-term RTIL permeation test (Δp=40 bar, T=50°C, t>400 hours) confirmed that there is no hydrodynamic flow through PTMSP for [Emim][DCA] and [Emim][BF_4]. The concept of CO_2 stripping from RTIL with the membrane contactor by the pressure (Δp=40 bar) and temperature (ΔT=20°C) swing was proofed by using PTMSP membrane and [Emim][BF_4]. The overall mass transfer coefficient value was equal to $(1.6\text{-}3.8)\cdot 10^{-3}$ cm/s with respect to liquid flow rate. By using the resistance-in-series model, it was shown that the membrane resistance contribution to the gas transfer was estimated to be approximately 8%.

Keywords: membrane contactor, room-temperature ionic liquid, PTMSP, carbon dioxide, stripping

1. Introduction

CO_2 stripping (desorption) from different absorbents plays a significant role in the absorption–desorption process to remove acid gases such as CO_2 from gas streams. An important emerging application of gas-liquid membrane contactors is focused on the regeneration of liquid CO_2 absorbents via stripping of dissolved CO_2 through the membrane (Zhao et al., 2016; Bazhenov and Lyubimova, 2016). Within this process transfer of CO_2 from the rich solvent to the gas phase is occurred, while the lean (regenerated) solvent is recycled for further absorption process.

A commonly used membrane contactors are the systems in which the porous membranes (pore size 0.1-0.3 μm) act as nonselective barriers to separate two phases. The hollow fiber membranes based on polytetrafluoroethylene (PTFE) (Khaisri et al., 2011; Ghadiri et al., 2013), polyvinylidenefluoride (PVDF) (Mansourizadeh and Ismail, 2011; Rahbari-Sisakht et al., 2013a), polysulfone (Rahbari-Sisakht et al., 2013b) were used for CO_2 stripping processes.

An important role in the both membrane CO_2 stripping and absorption plays a proper selection of liquid absorbent. It should possess high surface tension and negligible vapor pressure combined with high CO_2 sorption capacity. Room-temperature ionic liquids (RTILs), i.e. organic salts with melting temperatures less than 100°C, are among the best candidates that meet the stated criteria (Ramdin et al., 2012; Dai et al., 2016a).

A great variety of available organic/inorganic cations and anions allows to design RTILs with unique properties, which are widely studied as solvents, media or additives in catalysis (Hallett and Welton, 2011; Andreeva et al., 2007), electrochemical applications (MacFarlane et al., 2007), analytical (Sun and Armstrong, 2010) and biochemistry (Jain et al., 2005), membrane gas separation processes (Dai et al., 2016a; Akhmetshina et al., 2017) etc. Since RTILs might also possess relatively high CO_2 solubility and noticeable solubility selectivity over other gases, they were proposed for carbon dioxide capture and stripping as an alternative to conventional solvents due extremely low volatility, good thermal stability, lower heat duty at desorption stage as a result of physical bonding of CO_2 molecules, low corrosiveness and biodegradability (Ramdin et al., 2012, 2014; Lei et al., 2014; Karadas et al., 2010; Bazhenov et al. 2014). RTILs demonstrate typical behavior of a physical solvent in that the solubility of gases increases with gas pressure according to Henry's Law typically for gas pressures up to 10 bar (Dai et al., 2016a), thus the increasing of carbon dioxide partial pressure decreases energy requirements for RTILs as physical CO_2 solvents (Karadas et al., 2010). This results in greater potentials of RTILs in high-pressure applications (e.g. pre-combustion CO_2 capture or natural gas sweetening).

Imidazolium-based RTILs 1-ethyl-3-methylimidazolium ethylsulfate ([Emim][$EtSO_4$]) and 1-ethyl-3-methylimidazolium acetate ([Emim][Ac]) were already used for the CO_2 capture in the

gas-liquid contactors with porous hollow fiber membranes made from hydrophobic polypropylene (PP) or polysulfone (Albo et al., 2011; Gómez-Coma et al., 2014, 2016).

Sirkar et al. (2013, 2014) were the first who studied the applicability of RTILs with membrane contactors for high pressure and temperature pre-combustion CO_2 capture from syngas. They used porous ceramic tubes with silane coating and porous polyether ether ketone (PEEK) hollow fibers. Similarly, Dai and Deng (2016) and Dai et al. (2016b) applied porous glass membranes and butyl-3- methlyimidazolium tricyanomethanide ([Bmim][TCM]) to absorb CO_2 at high temperatures (up to 80ºC) and pressures (up to 20 bar).

The main problem in the operation of gas-liquid membrane contactors is the wetting of membrane pores, which leads to substantial increase of mass transfer resistance (Albo et al., 2011; Dai and Deng, 2016; Dai et al., 2016c). Wetting risk imposes restrictions on the pressure difference between the liquid and gas side of membrane contactor (typically of 0.2-0.3 bar) (Mosadegh-Sedghi et al., 2014). There are two ways to eliminate wetting effect and prevent any penetration of the solvent into the organic polymer membrane. The first method is to use a composite hollow fiber or an asymmetric skinned membrane. The alternative is to use a dense, self-standing polymeric membrane, highly permeable towards CO_2 and impermeable towards the solvent.

A thin selective layer coated onto a porous polymer support reduces the membrane permeability. However, the permeability loss can be compensated by the increasing the driving force with elevating the trans-membrane pressure. Recently, Nguyen et al. (2011) tested composite hollow fibers with a thin dense layer, based on a highly permeable glassy polymers (poly[1-(trimethylsilyl)-1-propyne] (PTMSP) and Teflon AF 2400), coated on a porous PP support for the absorption of CO_2 in conventional amine solutions. It has been found that the membrane with Teflon-AF thin layer shows the capture ratio and the overall mass transfer coefficient at a level of porous PP membrane. Dibrov et al. (2014) found that the thin film composite membrane with PTMSP layers on a metal-ceramic support demonstrated stable CO_2 flux during 100 h of stripping process from amine solution at elevated pressure and temperature (30 bar, 100 ^{0}C). Scholes et al. (2015) studied the CO_2 stripping from monoethanolamine solution using three composite membranes with a selective layer of PTMSP, PIM-1 and Teflon AF1600 on a porous PP support. It is found that over 90% of the overall resistance falls on the liquid boundary layer. Recently, thin film composite membrane approach was used for membrane absorption with RTIL solvent: Dai et al. (2016c) demonstrated the potential of applying the PP hollow fibers with dense Teflon AF 2400 layer for CO_2 capture at elevated temperatures (80°C) and pressures (20 bar) with [Bmim][TCM] as absorbent. The composite membrane contactor showed better long-term stability compared with the porous PTFE membrane contactor.

Integrally dense membrane contactor, i.e. the contactor based on non-porous self-standing membranes, is little used for CO_2 absorption/stripping. In cited article (Nguyen et al., 2011), a module based on self-standing polydimethylsiloxane (PDMS) hollow fibers were also tested. It has been experimentally found that these fibers showed lower performances in comparison to the porous and composite fibers. Nevertheless, both laboratory and pilot plant measurements on the separation of CO_2 from flue gas by Scholes et al. (2014) reports that the contactor based on non-porous PDMS does not experience wetting, yet the overall mass transfer coefficient two orders of magnitude less than the porous PP contactor.

Authors of papers (Dibrov et al., 2014; Trusov et al., 2011; Bazhenov et al., 2012; Shutova et al., 2014; Shalygin et al., 2008; Beggel et al. 2010; Volkov et al. 2015) examined the potential of dense membrane contactors based on disubstituted polyacetylenes, polynorbornene, polyvinyltrimethylsilane (PVTMS) for CO_2 stripping and absorption with various both chemical and physical absorbents. It was demonstrated that PTMSP, a polymer with the highest CO_2 permeability, is long-term stable and impermeable under elevated temperatures and pressures for the hydrodynamic flux of water (trans-membrane pressure Δp up to 100 bar, T up to 100°C) (Trusov et al., 2011; Grekhov et al., 2012), aqueous amine solvents (Δp up to 40 bar, T up to 100°C) (Trusov et al., 2011; Bazhenov et al., 2012). Moreover, this material turned out to be a barrier for RTIL 1-butyl-3-methylimidazolium tetrafluoroborate [Bmim][BF_4] (Δp=40 bar, T = 30 and 100°C) (Volkov et al. 2013). Therefore PTMSP can be considered as promising material for CO_2 stripping from RTIL as a solvent.

In the present work, we focused on the CO_2 stripping process from RTIL using integrally dense membrane contactor based on PTMSP membrane. It is known that RTILs may gradually dissolve some polymeric membranes. A careful choice of the RTIL as the solvent for CO_2 is therefore crucial for an efficient stripping process.

The first objective of this study is swelling tests among several commercially available RTILs in order to identify the liquid with lowest thermodynamic affinity to the polymer, i.e. with the lowest swelling of the polymeric membranes. The second one is to investigate the CO_2 stripping flux and efficiency in flat-sheet dense membrane contactor based on PTMSP and to estimate the relative contribution of the membrane resistance to the overall mass-transfer process.

2. Experimental part

2.1. Ionic liquids

Eight different room-temperature ionic liquids with a varied characteristics were purchased from Sigma Aldrich Chemie GmbH: 1-Ethyl-3-methylimidazolium dicyanamide ([Emim] [DCA],

Aldrich #713384), 1-Ethyl-3-methylimidazolium tetrafluoroborate ([Emim][BF_4], Aldrich #711721), 1-Ethyl-3-methylimidazolium diethyl phosphate ([Emim][DEP], Aldrich #713392), 1-Butyl-3-methylimidazolium bis(trifluoromethylsulfonyl)imide ([Bmim][Tf_2N], Aldrich #711713), 1-Butyl-3-methylimidazolium tetrafluoroborate ([Bmim][BF_4], Aldrich #711748), trihexyltetradecylphosphonium dicyanamide ([P66614][DCA], Aldrich # 56776), trihexyltetradecylphosphonium bromide ([P66614][Br], Aldrich # 96662), trihexyltetradecylphosphonium bis(2,4,4-trimethylpentyl)phosphinate ([P66614][Phos], Aldrich # 28612). The 1-hexyl-3-methylimidazolium tetracyanoborate ([Hmim][TCB]) was provided by Merck KgaA, Germany. All the RTILs were used without further chemical purification. The only precaution taken was the dry storage under vacuum and elevated temperature (80°C) conditions to avoid any water uptake by the ionic liquid. Water content of used RTILs, after drying, was measured by Karl Fischer titration (Metrohm 756 KF Coulometer) and did not exceed 1300 ppm. The chemical structures and some properties of selected RTILs are listed in Table 1.

Table 1

Chemical structures and molar weights of studied ionic liquids.

Name	Chemical structure	MW, g/mole
[Emim][DCA]	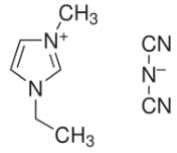	177.2
[Emim][BF_4]	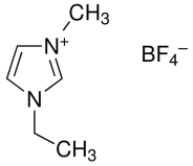	198.0
[Emim][DEP]	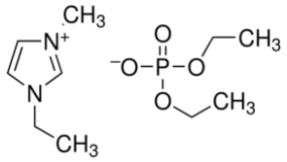	264.2
[Bmim][BF_4]	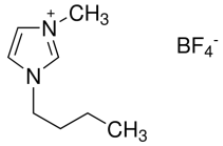	226.0

[Bmim][Tf_2N]	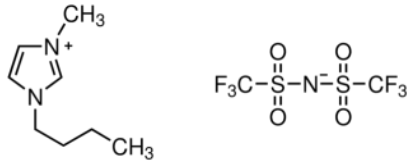	419.4
[Hmim][TCB]	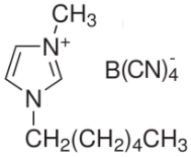	282.1
[P66614][DCA]	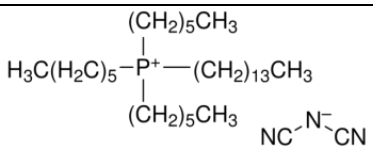	549.9
[P66614][Br]	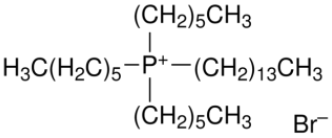	563.8
[P66614][Phos]	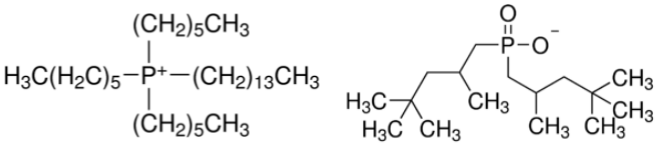	773.3

2.2. Membrane preparation

Poly[1-(trimethylsilyl)-1-propyne] (PTMSP) was synthesized by polymerization of 1-(trimethylsilyl)-1-propyne in a toluene solution using $TaCl_5$, with cocatalyst triisobutylaluminum (TIBA), as the catalyst (Khotimsky et al., 2003). The dense membranes (films) with required thickness were cast from solution with a polymer concentration of 0.5 wt.% (solvent: chloroform) onto a commercial cellophane. Then the cast film was covered with a Petri dish and left for slow evaporation for several days, followed by drying in the oven at 40°C until a constant sample weight was obtained. Further treatment of all membranes was according to the standard protocol of membrane preparation (Volkov et al., 2002). The membrane thickness was measured by a Mitutoyo® 273 Quick Step electronic micrometer.

2.3. Sorption and swelling experiments

Dense membrane samples with thicknesses of 60-75 μm were used for the sorption and swelling tests in RTILs. The dry preweighed rectangular polymer films (25×40 mm) were immersed and soaked in chosen RTILs at ambient temperature (22±2°C) within sealed bottles. Since the diffusivity of viscous RTILs in the polymer films might be a very slow process, the sorption/swelling experiments were carried out for at least 40 days to ensure reaching the

equilibrium. The samples were periodically removed from the RTILs, blotted with filter paper for the removal of the liquid excess from the surface and weighed in stoppered bottles to obtain a constant weight. After the experiments, the dimensions and weight of cleaned films were measured.

The sorption value has been expressed as a relative weight increase, $\Sigma = (m - m_0)/m_0$ where m is the polymer film weight after soaking and removal of RTIL excess from the surface, m_0 is the weight of the dry sample. The sorption value was measured with an experimental error of about 1% using a precision microbalance which allows the weighing of polymer samples with an accuracy of about 30 μg.

The polymer volumetric swelling degree (*SD*) in the RTILs was calculated as $SD = (Al/A_0 l_0) - 1$, where l and A are the thickness and surface area of the polymer film in the solvent, and l_0 and A_0 are counterparts for the dry film. The swelling degree was measured with an experimental error of about 5%.

2.4. FTIR spectroscopy

The PTMSP films soaked in selected RTILs were studied with FTIR spectroscopy. FTIR spectrometer IFS-66 v/s vacuum Bruker was used to collect spectra of dry polymeric films with a thickness of 8-10 μm and ionic liquids in transmission mode in the range of 400–4000 cm^{-1} (30 scans, resolution 2 cm^{-1}). The ionic liquid was placed between two optical silica glasses. The spectra of the soaked polymeric films containing ionic liquids were collected in the reflection mode (ATR) in the range of 600-4000 cm^{-1} by using IR microscope HYPERION-200 (150 scans, resolution 2 cm^{-1}, ZnSe crystal).

2.5. CO_2 and RTILs permeation testing

CO_2 permeability through PTMSP was determined by the volumetric method (Dibrov et al., 2014) at 30°C as $J \cdot l/\Delta p$ where J denotes the gas flux per unit surface area of the membrane, per unit time, Δp – transmembrane pressure, l – membrane thickness. Hydrodynamic permeation (leakage) of RTILs across the membrane was studied at a trans-membrane pressure of 40 bar and temperature of 50°C for at least 400 hours. The experiments were performed according to the procedure described earlier (Trusov et al., 2011): the flat-sheet sample of the tested membrane was placed in a dome-shaped dead-end filtration cell; then, the upper compartment of the cell was partially filled with the selected RTIL and pressurized with carbon dioxide. A porous stainless

steel support was used to avoid damage to the membrane due to the high pressure. Both cell and permeate collectors were kept in the thermal chamber.

2.6. CO_2 stripping from RTIL in membrane contactor

Stripping of CO_2 from the ionic liquid [Emim][BF_4] in a membrane contactor based on PTMSP dense membranes was carried out with the lab-scale high pressure/temperature membrane gas stripping set-up (Fig. 1) described previously (Shutova et al., 2014). The RTIL was initially saturated with carbon dioxide at a pressure of 10 bar. For this purpose, the absorber *3* was filled up with RTIL from the initial tank *1*. The absorber *3* is a high-pressure temperature-controlled vessel equipped with a propeller stirrer and encased in thermal chamber *4*. CO_2 entered the absorber *3* from the gas cylinder *2* and dissolved in the RTIL with constant agitation rate under the pressure 10 bar (controlled with Bronkhorst® precise pressure sensors) and temperature 30°C during at least 4 h to reach the equilibrium. Then, the saturated RTIL under the same pressure was supplied into the slit rectangular channel formed between the flat-sheet membrane and the shell within the membrane contactor *6*, which is schematically shown on Fig.2. The height of the slit channel is equal to 0.01 cm. The active membrane area in the contactor is 16 cm^2; the membrane thickness is 21±1 µm. A porous stainless steel support with negligible gas flow resistance was used in the permeate collector to prevent membrane damage. The membrane contactor is encased in thermal chamber 5 to control the process temperature. A stainless steel pipe (Swagelok, OD = 3 mm) with a length of about 1.5 m was installed in the thermal chamber *5*, just before the membrane contactor *6*, as a heat exchanger.

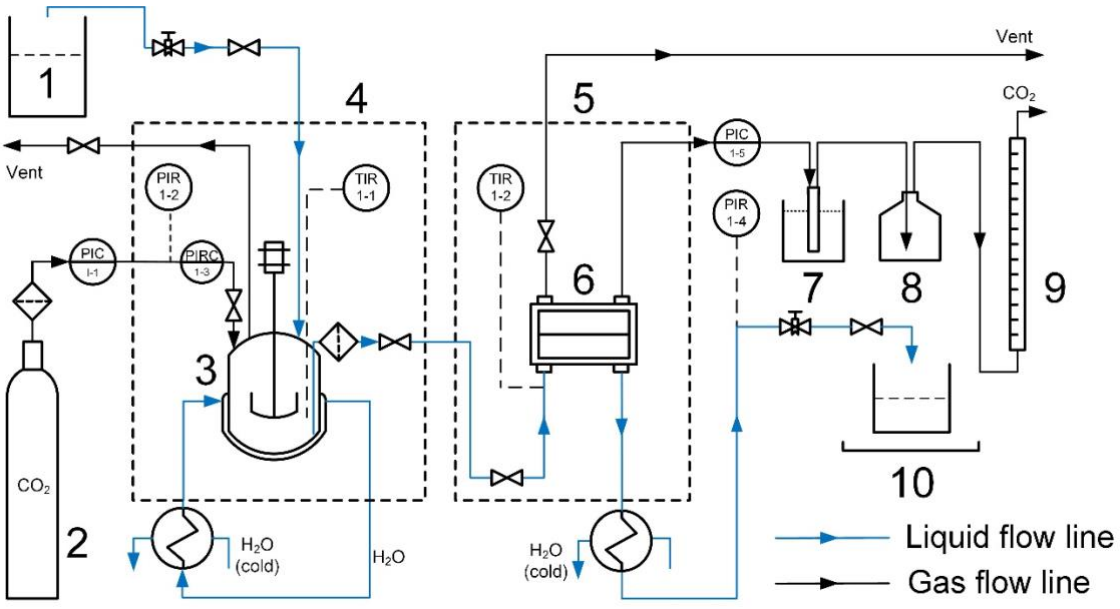

Fig. 1. Membrane gas stripping setup: *1* – initial ionic liquid tank; *2* – CO_2 gas cylinder; 3 – absorber; *4*, *5* – thermal chambers; *6* – high-pressure flat-sheet gas-liquid membrane contactor; *7* – cold trap; *8* – safety flask; *9* – digital gas flow meter; *10* – degassed ionic liquid sampler and microbalance.

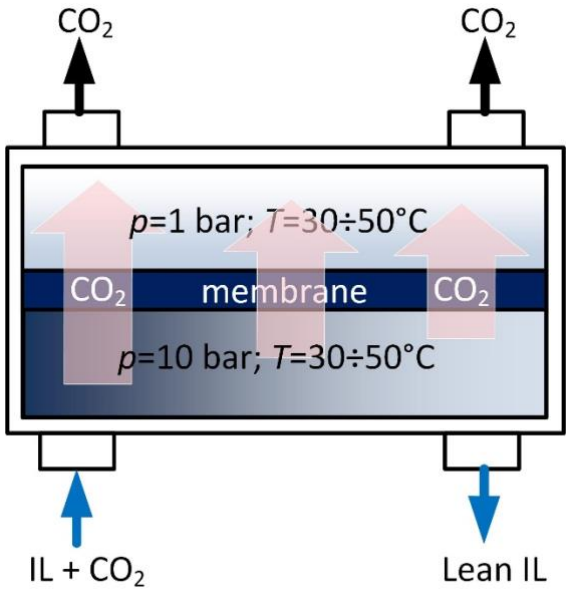

Fig. 2. Scheme of high-pressure flat-sheet gas-liquid membrane contactor.

During the stripping process, CO_2 was desorbing from the RTIL through the membrane to the permeate collector of the contactor which is at atmospheric pressure. During the experimental run, the CO_2 flow was leaving the permeate compartment of the contactor, and its flow rate was directly measured with the flow-meter *9*. The RTIL flow rate in the contactor was adjusted with a needle valve at the outgoing liquid flow line. The liquid flow rate was estimated through the weighing of the degassed ionic liquid collected in the sampler *10* with an electronic microbalance followed by dividing this value by the RTIL density. During the experiments, the desorbed CO_2 flow was measured as a function of RTIL flow-rate. It should be noticed that during the whole operation of gas-liquid membrane contactor, no droplets of RTIL was observed in the gas collector of the contactor.

3. Mass transfer in membrane contactor

The key characteristics of gas mass transfer are the stripping flux and the stripping efficiency. The latter parameter is defined as

$$\eta = 1 - C_{\mathrm{L}}^{\mathrm{out}} / C_{\mathrm{L}}^{\mathrm{in}} \qquad (1)$$

where C_L^{out} and C_L^{in} are the feed liquid phase CO_2 concentrations at outlet and inlet of the membrane contactor, respectively. The CO_2 stripping flux J_{CO_2} is equal to the mass loss of the gas under liquid flow through the slit channel per membrane area *A*, per unit time:

$$J = \frac{Q_L}{A}\left(C_L^{in} - C_L^{out}\right) = \frac{Q_L}{A} C_L^{in} \eta \qquad (2)$$

where Q_L (cm^3/s) is the liquid flow rate.

The CO_2 stripping flux was measured at different liquid flow rates, and the stripping efficiency η was calculated from the Eq. (2).

Similar to the absorption process, mass transfer resistance in stripping can also be predicted by the resistance-in-series model, which considers the resistances from the membrane and liquid and gas boundary layers. However, CO_2 transfer direction is reversed from the liquid phase to the gas phase under the driving force of CO_2 concentration or partial pressure difference across the membrane.

To define the overall mass transfer coefficient (MTC), we use the known approach, also used for gas absorption simulation in membrane contactors (Sirkar, 1992; Cussler, 1994). In virtue of the mass balance of CO_2 in the liquid/gas stripper (the system is assumed to be under steady state conditions), the flux in Eq. (2) must be equal to the average flux of CO_2 across the membrane ("average" means flux averaging over the length of the channel). This flux can be represented by two equivalent ways: through overall MTC based on liquid phase (k_{ov}) or through that ($k_{ov}^{(g)}$) based on gas phase concentrations:

$$J = k_{ov} \cdot \overline{\Delta C} \qquad (3a)$$

$$J = k_{ov}^{(g)} \cdot \overline{\Delta p} \qquad (3b)$$

Here $\Delta C = C_{L(feed)} - C_{L(perm)}$ is the concentration difference of the gas in bulk feed solution and the equilibrium concentration of gas in a hypothetical liquid permeate; $\Delta p = p_{feed} - p_{perm}$ is the CO_2 partial pressure drop between feed and permeate; bars above quantities denote averaging over the length of the channel. Eq. (3) assumes that mass transfer coefficients do not depend on the concentration (pressure).

The equilibrium concentration of a penetrant gas dissolved in a liquid feed and hypothetical liquid permeate can be related to the pressure of the gas by the relation $C_L = S\,p$. We assume that

the gas solubility coefficient S is a constant in the pressure range up to 10 bar. Then two MTCs are interconnected as

$$k_{ov}^{(g)} = Sk_{ov} \tag{4}$$

As shown in (Cussler, 1994), $\overline{\Delta C}$ is the logarithmic mean concentration differences of CO_2 in the liquid at the inlet and outlet from the membrane contactor. Given that the gas concentration in the permeate does not vary with module length, we obtain:

$$\overline{\Delta C} = \frac{\Delta C^{in} - \Delta C^{out}}{\ln\left(\Delta C^{in}/\Delta C^{out}\right)} = -\frac{C_L^{in}\eta}{\ln\left(1-\eta/(1-\gamma)\right)} \tag{5}$$

where $\gamma = C_{L(perm)}/C_L^{in} = p_{perm}/p_{feed}$. As partial permeate pressure is significantly lower than that of CO_2 pressure over the liquid entering the membrane contactor, the γ value can be neglected. Then Eqs. (2) and (3a) taking into account Eq. (5) gives the following expression for the overall MTC:

$$k_{ov} = -\frac{Q_L}{A}\cdot\ln\left(1-\eta\right) \tag{6}$$

According to resistance-in-series approach, the overall resistance $R = 1/k_{ov}$ to gas transfer through the membrane can be expressed as the sum of the resistances associated with each phase: feed, membrane, and permeate. Using the assumption that the stagnant boundary layer occurs only on the feed side of the membrane, i.e. neglecting the gas-phase resistance, we have

$$\frac{1}{k_{ov}} = \frac{1}{k_L} + \frac{1}{k_m} \tag{7}$$

It is necessary to emphasize the difference of gas mass transfer from the liquid phase to gas phase across porous and nonporous membranes. In the case of a porous membrane, two transfer modes are possible: (1) non-wetted where the membrane pores are gas-filled, and (2) wetted mode where the membrane pores are liquid-filled. In the case of a non-porous (dense) membrane considered in this study, the gas transport through the membrane can be described with the solution-diffusion mechanism.

The liquid feed mass transfer coefficient k_L can be expressed via the gas diffusivity D across the boundary layer with thickness δ, i.e. $k_L = D/\delta$; the membrane mass transfer coefficient (the membrane's permeance) k_m could be written as $k_m = D_m K/l_m$ where D_m is the diffusion coefficient of the gas through the membrane with thickness l, K is the partition coefficient of CO_2 from the feed solution into the membrane (Cussler, 1994). This partition coefficient can be written as the ratio of the solubility coefficients of CO_2 in the membrane and feed liquid solution

$$K = S_{\mathrm{m}} / S \tag{8}$$

where $S_{\mathrm{m}} = C_{\mathrm{m},i} / p$, $S = C_{\mathrm{L},i} / p$; $C_{\mathrm{m},i}$ is the concentration of CO_2 in the membrane at the feed liquid–membrane interface, $C_{\mathrm{L},i}$ is the concentration of CO_2 in the feed liquid-phase at this interface.

In view of the above, the overall resistance will be as follows:

$$R \equiv \frac{1}{k_{\mathrm{ov}}} = \frac{\delta}{D} + \frac{l_{\mathrm{m}} S}{P_{\mathrm{m}}} \tag{9}$$

Dividing this equation by gas solubility coefficient S, we get the overall resistance based on gas phase:

$$R^{(g)} \equiv \frac{1}{k_{\mathrm{ov}}^{(g)}} = \frac{\delta}{P} + \frac{l_{\mathrm{m}}}{P_{\mathrm{m}}} \tag{10}$$

where $P = DS$ and $P_{\mathrm{m}} = D_{\mathrm{m}} S_{\mathrm{m}}$ are the permeability coefficients of CO_2 in the feed boundary layer and the membrane, respectively. If the permeability coefficients are expressed in barrers (1 barrer = 10^{-10} $cm^3(STP)\cdot cm/(cm^2\cdot s\cdot cmHg)$) and the thickness is in microns, then the dimension of the overall resistance $R^{(g)}$ is GPU^{-1} (1 GPU = 10^{-6} $cm^3(STP)/(cm^2\cdot s\cdot cmHg)$).

4. Results and discussion

4.1. Interaction of RTILs with PTMSP

Table 2 presents the sorption and swelling data of PTMSP in chosen ionic liquids. From data obtained one can conclude that: (1) there is no clear dependence between viscosity and sorption values; (2) a linear correlation between RTIL surface tension and sorption can be defined – the lower surface tension, the higher the liquid sorption value (except two first imidazolium-based RTILs). The same reverse dependence was observed earlier for both binary water-ethanol solvents and conventional physical CO_2 capture solvents (propylene carbonate, dimethyl ethers of poly(ethylene glycole)) (Volkov et al., 2013). PTMSP demonstrated a higher solvent uptake and a swelling degree in bulky [P66614][Phos] (MW 773.3) and [P66614][Br] (MW 563.8) liquids which are characterized by low surface tension. At the same time, highly polar RTILs with high surface tension ([Emim][DCA] and [Emim][BF_4]) demonstrate a minimum sorption in the PTMSP. Thus, these two liquids which exhibit low thermodynamic affinity to the polymer, are suitable candidates for application in gas-liquid membrane contactor systems.

Table 2

Sorption and swelling degree of PTMSP in studied RTILs. The surface tensions and viscosities of liquids are also presented (data taken from Ionic Liquids Database - ILThermo (v2.0), Accessed July 07, 2016; T=25°C and p=101.325 kPa).

RTIL	η, mPa·s	σ, mN/m	Sorption, g/g	Swelling degree, %
[Emim][DCA]	14.5	60.3	0.02	0*
[Emim][BF_4]	36.9	54.0	0.02	0*
[Bmim][BF_4]	99	44.4	0.79	21
[Hmim][TCB]	49.8	41.1	1.04	44
[Emim][DEP]	457	35.9	1.35	54
[Bmim][Tf_2N]	50.7	33.0	1.74	57
[P66614][DCA]	439	32.3	1.80	108
[P66614][Br]	2988	29.3	2.11	123
[P66614][Phos]	1402	28.2	2.19	139

*The values obtained are within the measurement accuracy

The interactions of RTILs with the PTMSP were also evaluated by FTIR spectroscopy. For this purpose, the PTMSP films after sorption/swelling experiments with RTILs were used. Two liquids with a high surface tension ([Emim][DCA], [Emim][BF_4]) and the two liquids with low surface tension ([P66614][Br], [P66614][Phos]) have been chosen.

The reflection spectra for swollen PTMSP, and also spectra for pure PTMSP and RTILs are shown in Fig. 3 and 4. The weak bands in the range of 2100-2200 cm^{-1} from valence vibrations of the $[DCA]^-$ anion nitrile groups in the PTMSP-[Emim][DCA] spectrum (Fig. 3a) indicate RTIL presence in the polymer film; however, its concentration in the polymer is very small. The detailed consideration of the spectrum in Fig. 3a shows some changes of absorption bands for both the polymer and RTIL. The 828, 910 and 683 cm^{-1} bands associated with the valence vibrations of Si-C bonds in the polymer and remain without any noticeable changes in PTMSP-solvent sample. The 747 cm^{-1} band is responsible for complex oscillative motion in PTMSP. This band not only shifts towards short waves but also loses splitting which is typical for the polymer having mixed microstructure (*cis-trans*). The described spectrum features for such a rigid polymer as PTMSP can be related to the symmetry breaking in the polymeric unit, accompanied by a change in the

backbone conformation. Detectable changes influenced by [Emim][DCA] occur in the polymer spectrum in the region of the C=C bond valence vibrations (1540-1580 cm^{-1}). Three bands, characteristic for the double bond in the PTMSP unit, and one band derived from skeletal vibrations in the [Emim][DCA] cation imidazole ring, merge into one wide band in the soaked polymer spectrum. Significant changes in the imidazole ring structure are also observed, namely, bands intrinsic to the =CH bonds vibrations in the ring (3100-3200 cm^{-1}) have totally disappeared. This suggests that the aromaticity of RTIL cation was strongly affected by polymer-RTIL interaction. Fig. 3b shows the PTMSP-[Emim][BF_4] spectrum compared to that of PTMSP and [Emim][BF_4]. The RTIL content in the polymer also marginally. The polymer spectrum undergoes almost the same changes as those in the case of [Emim][DCA]; significant changes are observed in the region of double bonds and bands, sensitive to chain conformation.

Fig. 4 shown the spectra of PTMSP with phosphonium-based RTILs: [P66614][Br] and [P66614][Phos]. The spectra show a higher liquid content in the polymer compared with the aforementioned liquids. Amount of [P66614][Br] in PTMSP (Fig. 4a) is lower than that of [P66614][Phos] (Fig. 4b), which is in agreement with sorption data. In the case of [P66614][Br], $[Br]^-$ anion does not have intrinsic bands in FTIR spectrum. The particular intensity of phosphonium-based compounds bands is observed in the spectra for PTMSP film soaked in [P66614][Phos] (Fig. 4b). In this spectrum, considerably intensive bands of the RTIL strongly shifted towards the long-wave region: the P=O band of the RTIL anion 1166 cm^{-1} shifts to 1148 cm^{-1} and the P-CH_2 band of the RTIL 738 cm^{-1} shifts to 718 cm^{-1}.

Analysis based on quantum chemical calculations shows that =C-Si bond in the monomeric unit of PTMSP is strongly polar: a high positive charge (1.190 e) occurs on the silicon atom, and a significant negative charge (-0.363 e) occurs on the carbon atom at double bond [Legkov et al., 2012]. Given this, it can be assumed that the interaction of the RTIL with the polymer occurs due to the coordination of the cation and the anion of the RTIL towards oppositely charged PTMSP atoms. This interaction is accompanied by a change in the conformation of the chain and redistribution of the electron density in the -C=C-$SiMe_3$ unit.

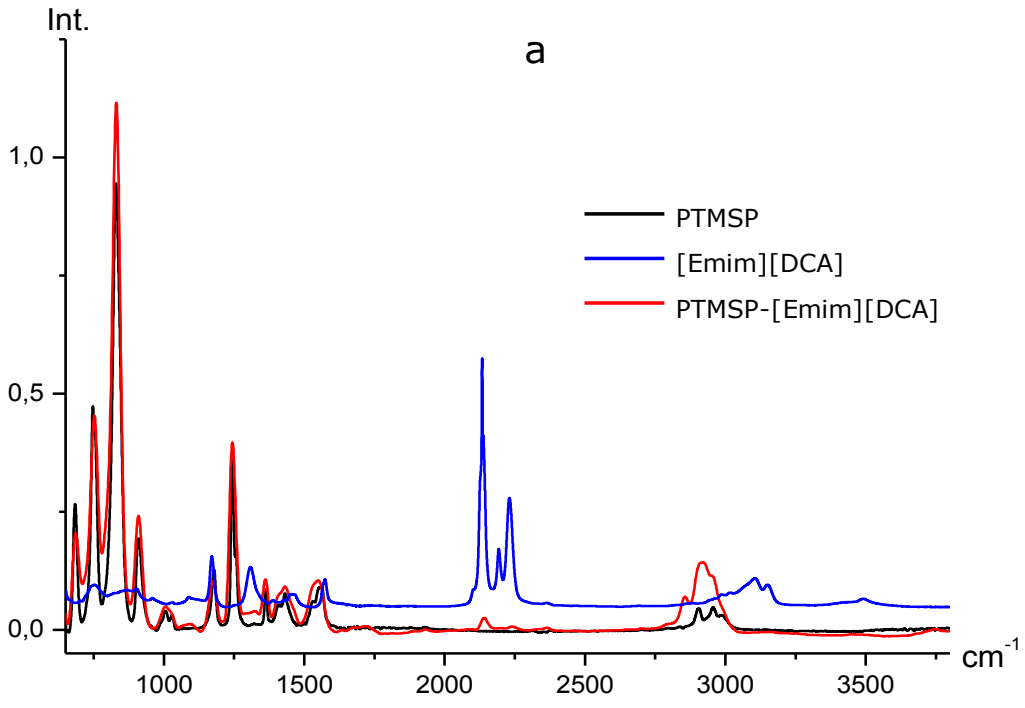

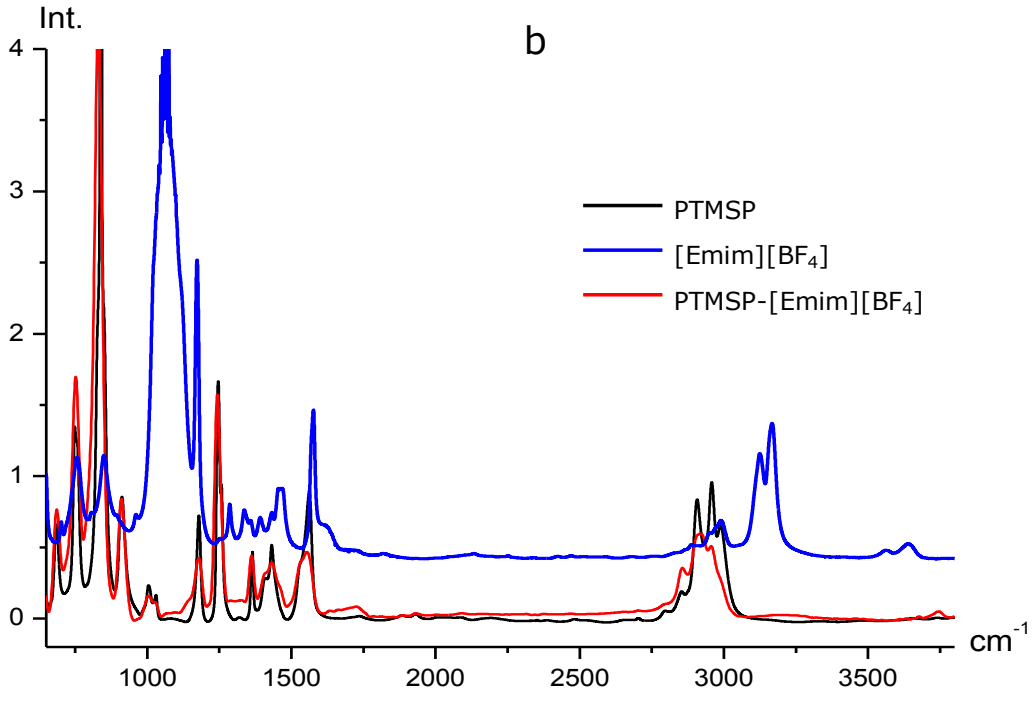

Fig. 3. FTIR spectra of swollen film of PTMSP in ionic liquids: [Emim][DCA] (a) and [Emim][BF_4] (b). Spectra of pure PTMSP and individual liquids are also shown.

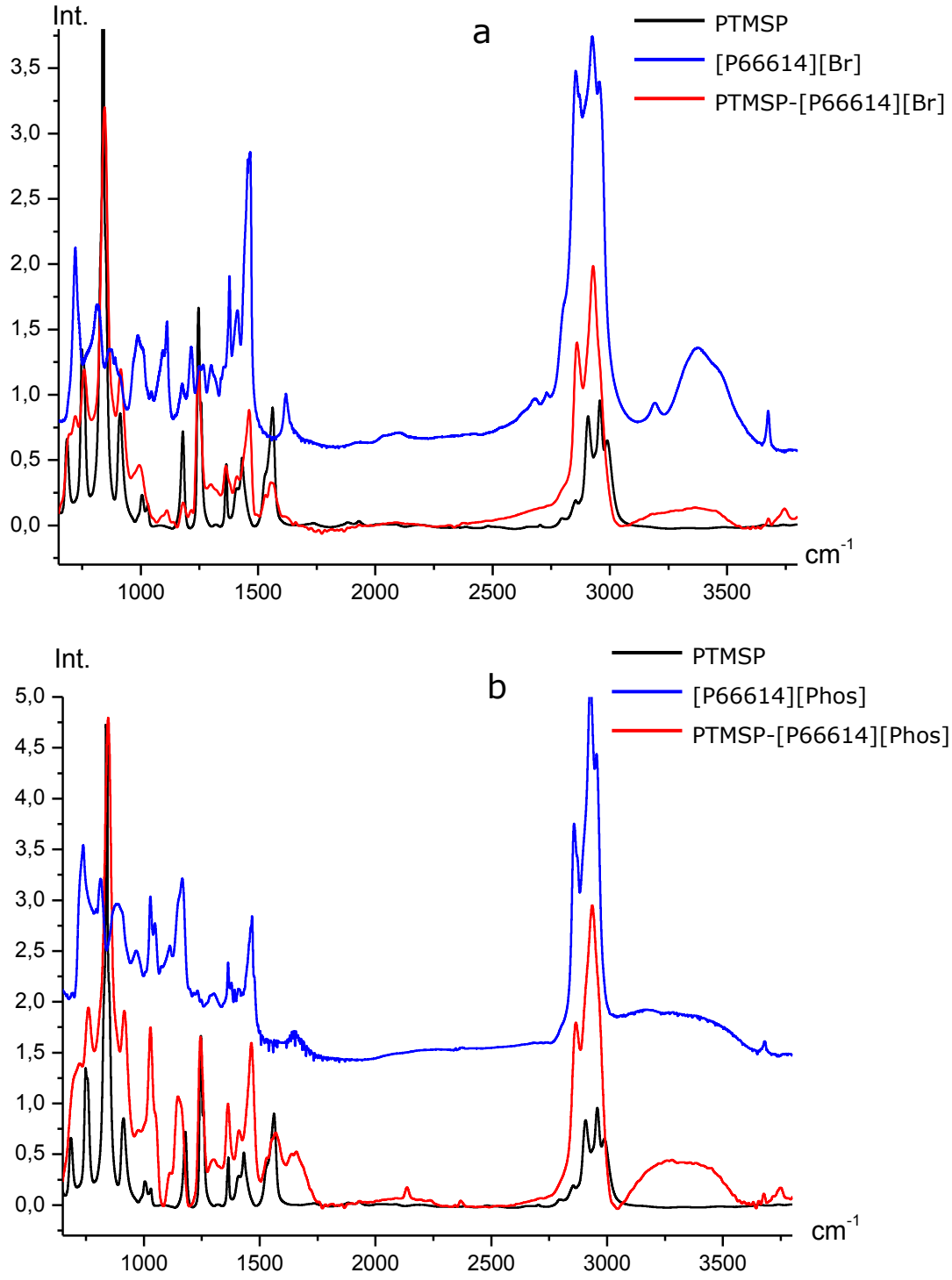

Fig. 4. FTIR spectra of swollen film of PTMSP in ionic liquids: [P66614][Br] (a) and [P66614][Phos] (b). Spectra of pure PTMSP and individual liquids are also shown.

FTIR data testify that phosphonium-based RTILs interact with PTMSP significantly higher than imidazolium-based ones; this manifests itself in a higher concentration of first type RTILs in the polymer compared with second type ones.

As was shown above (Table 2), sorption of phosphonium-based RTILs in PTMSP is one order of magnitude higher than that for imidazolium-based RTILs. Thus, the conclusions obtained from FTIR spectroscopy data are consistent with the results of sorption measurements.

Following on from the results of sorption and FTIR data, it is reasonable to expect that PTMSP might possess barrier properties towards [Emim][DCA] and [Emim][BF_4] and be permeable for [P66614][Br] and [P66614][Phos]. The membrane leakage testing with chosen RTILs confirmed these expectations. Taking into account the high viscosity of ionic liquids and possible change of their macroscopic properties as a result of CO_2 loading, the membrane cell was pressurized by carbon dioxide and continuously kept under the operating pressure during at least 400 hours. No hydrodynamic flow of [Emim][BF_4] or [Emim][DCA] through PTMSP membranes was visually observed during these leakage tests. At the same time, the experiment showed the absence of PTMSP barrier properties toward phosphonium-based RTILs: the visual study showed the presence of RTIL leakage through the PTMSP membranes after approx. 220-260 h of testing. Earlier it was shown for PTMSP/water/ethanol system (Volkov et al., 2013; Yushkin et al., 2015) that surface tension has a significant effect on the appearance of hydrodynamic permeability of the polymer and, hence, the applicability of this membrane material in high-pressure gas-liquid contactors. It was also recently estimated (Filippov et al., 2015) that the critical entry pressure, i.e. the trans-membrane pressure at which liquid penetrates into the pores of the membrane, of water-ethanol mixtures in PTMSP might reach 100 bar or even higher for the solutions with a surface tension of 50 mN/m or higher. This estimation is in a good agreement with our finding that PTMSP is impermeable at transmembrane pressures up to 40 bar for [Emim][DCA] and [Emim][BF_4] having $\sigma > 50$ mN/m. It should be noted that porous membranes commonly used in gas-liquid contactors become wetted and permeable at much lower pressure. For example, in the case of PTFE membranes, the critical entry pressure is lower than 3 bar for water-ethanol solvents with $\sigma > 50$ mN/m (Dindore et al., 2004). Such advantage of the dense membranes over hydrophobic porous membranes provide greater flexibility in selection of CO_2 solvents especially for high-pressure applications such as pre-combustion or natural gas sweetening.

4.2. CO_2 stripping from the RTIL in membrane contactor

The proof of principle of high-pressure gas-liquid membrane contactor for CO_2 stripping from RTIL solvent was verified by using [Emim][BF_4] and the flat-sheet PTMSP membrane. From the pair [Emim][BF_4] and [Emim][DCA] the first one was chosen based on literature data for CO_2 solubilities: CO_2 sorption capacity of [Emim][BF_4] is higher than that of [Emim][DCA], which is

depicted by a lower value of Henry's law constant, 3.0465 MPa (Soriano et al., 2008) and 9.5955 MPa (Camper et al., 2005) at 40ºC, respectively.

The dense PTMSP membrane separates the two phases within the gas-liquid contactor: feed solution of CO_2 in the ionic liquid at 10 bar as in the absorber and permeate gas phase under the atmospheric pressure. Sweep gas or vacuum was not used, so, permeate constituted a stagnant gas layer. CO_2-saturated RTIL [Emim][BF_4] is convected parallel to the membrane surface through the rectangular channel with the cross-sectional area $A_{ch} = Lh$ (channel height $h = 0.01$ cm and channel length $L = 4$ cm), carbon dioxide diffuses through the membrane and then desorbes to the permeate collector of the contactor. Inlet concentration of the gas in [Emim][BF_4] on the channel is equal to the equilibrium one at CO_2 pressure of 10 bar and a temperature of 303 K within the absorber. At these *p* and *T* conditions this concentration is 0.43 mol/kg RTIL or 0.54 mol/L (molar fraction is 7.6%) (Soriano et al., 2008).

Fig. 5 shows the results of CO_2 stripping from [Emim][BF_4] as a function of liquid flow-rate. CO_2 stripping flux was measured directly in the experiment at different flow-rates; the stripping efficiency was further calculated from CO_2 stripping flux data with Eq. (2).

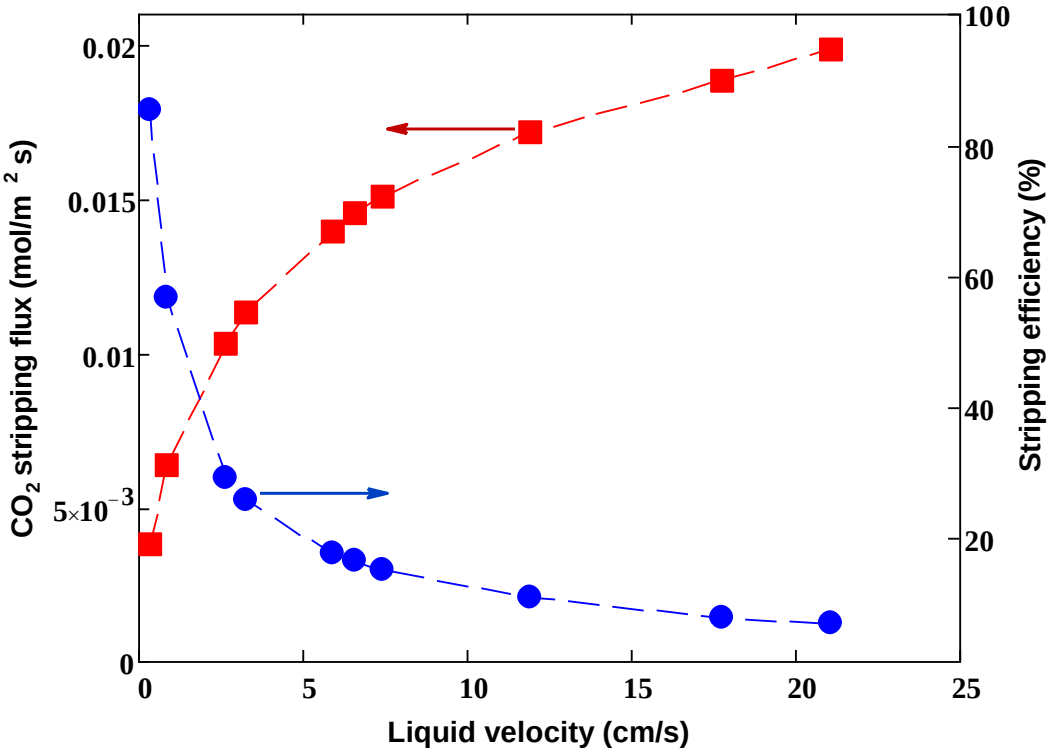

Fig. 5. The stripping efficiency and CO_2 stripping flux vs. the liquid velocity. The liquid velocity $u = Q_L/A_{ch}$ where A_{ch} is the cross-sectional area of the liquid channel, temperature and trans-membrane pressure in the contactor are 30°C and 10 bar.

As can be seen from Fig. 5, CO_2 stripping flux increased with the liquid velocity, while the efficiency decreases (trade-off between J and η). It is evident that a slower liquid velocity leads to an increase in residence time of solvent in slit channel of membrane contactor and, consequently, to higher values of η. As flux is proportional to the product of Q_L and η, the flux increases with the liquid velocity with a gradually decreasing slope. A similar behavior was observed, particularly, in Ref. (Khaisri et al., 2011). The trade-off between the flux and the efficiency assumes that $J \times \eta$ function passes through a maximum. A simple estimation shows that the maximum of the product of J and η is achieved at the liquid velocity of about 1.2 cm/s. In this context, this is the preferable liquid solution velocity for the system investigated. At this velocity, $\eta \approx 48\%$ and $J = 0.0074$ mol/(m^2 s) (1.2 kg/m^2 h). It should be noted that this value is two orders of magnitude higher than that obtained for membrane contactor based on porous polypropylene hollow fibers with analogous imidazolium-based IL – [Bmim][BF_4] (maximal value ~3.5×10^{-5} mol/(m^2 s), see Lu et al., 2014).

Calculation based on Eq. (6) showed that overall MTC increases with an increase in liquid velocity from $1.6\cdot10^{-3}$ cm/s at $u = 0.33$ cm/s to $3.8\cdot10^{-3}$ cm/s at $u = 21$ cm/s (Fig. 6). Solubility coefficient of CO_2 in [Emim][BF_4] is equal to $S = 0.054$ mmol/(cm^3·bar) or 0.016 cm^3 (STP)/(cm^3·cm Hg) at 303 K, as it follows from Ref. (Soriano et al., 2008). Consequently, overall MCT based on gas phase $k_{ov}^{(g)} = S k_{ov}$ ranges within 25-61 GPU. Comparison of calculated overall MTC with available literature data for membrane contactors with analogous imidazolium-based ILs shows that MTC is also higher in our case: $(1.1\text{-}3.2)\times10^{-4}$ cm/s for [Emim][Ac] and 0.7×10^{-4} cm/s for [Emim][$EtSO_4$] within membrane contactor with polypropylene hollow fibers (Gómez-Coma et al., 2014); $(0.365\text{-}1.01)\times10^{-4}$ cm/s for [Bmim][TCM] within membrane contactor with tubular glass membranes (Dai et al. (2016)); $(2.4\text{-}3.7)\times10^{-4}$ cm/s for [Emim][Ac] within membrane contactor with polysulfone hollow fibers (Gómez-Coma et al., 2016); $(0.9\text{-}1.67)\times10^{-3}$ cm/s for [Bmim][DCA] within membrane contactor with polypropylene hollow fibers (Mulukutla et al., 2014). Almost all the compared works used contactors with porous membranes which can suffer from the wetting effect resulted in lower overall MTCs. An exception is the latter publication where authors used PP hollow fibers with thin plasma polymerized hydrophobic porous fluorosiloxane coating on the outer surface of the fiber: overall MTC is comparable with ours.

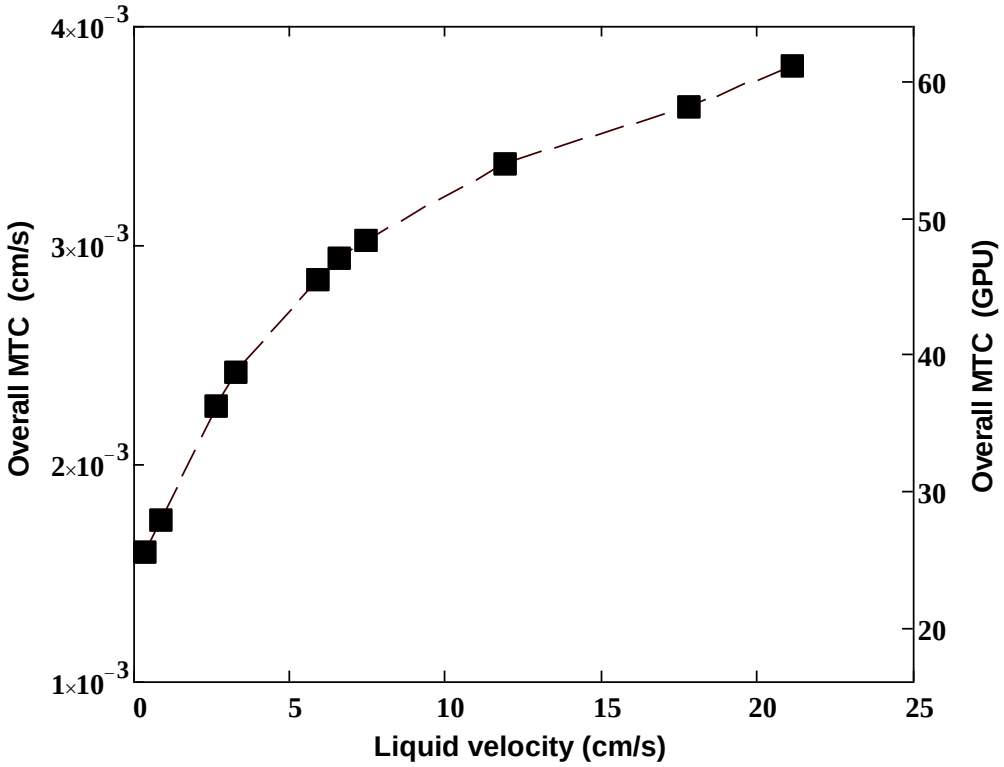

Fig. 6. The overall MTC for CO_2 stripping from [Emim][BF_4] in the PTMSP-based flat-sheet membrane contactor as a function of the liquid velocity; temperature and trans-membrane pressure in the contactor are 30°C and 10 bar.

As defined above (Eq. (10)), the overall resistance to gas transfer is the sum of the resistances associated with the liquid phase and the membrane.

The question arises, which of the contributions into the overall resistance dominates – the membrane resistance $R_m = l_m / P_m$ or the liquid layer resistance $R_L = \delta / P$. The permeability of the PTMSP membrane, containing ionic liquid, can be approximated by the series model:

$$\frac{1}{P_m} = \frac{\phi}{P} + \frac{1-\phi}{P_p} \qquad (11)$$

where ϕ is the volume fraction of the RTIL in the membrane, P_p is the permeability of the pure polymeric membrane. It should be noted that the series model gives a lower bound for permeability compared to that in other models for binary polymer systems (Robeson, 2010). So, in the absence of experimental data for permeability of the polymer/ionic liquid membrane, the use of approximation (11) will give an *upper estimate* for the membrane resistance. Furthermore, the membrane thickness change due to its swelling should be taken into account. The thickness of the swollen membrane l_m is related to the thickness of dry membrane l as $l_m = l(1-\phi)^{n-1}$ where

$n = 2/3$ in the case of isotropic swelling and $n = 0$ for fully anisotropic swelling (Bitter, 1984). Under the conditions of stripping experiments, the membrane is assumed to swell only in the direction that is perpendicular to the membrane surface due to its confinement on the support, therefore the relation can be adopted as follows:

$$l_{\mathrm{m}} = l/(1-\phi) \tag{12}$$

On substituting Eqs. (11) and (12) into Eq. (10), we obtain the following:

$$R^{(g)} = R_{\mathrm{L}} + R_{\mathrm{m}} = \frac{\delta}{P} + \frac{l}{P_{\mathrm{p}}}\beta \tag{13}$$

where $\beta = 1 + \frac{\phi}{1-\phi}\frac{P_{\mathrm{p}}}{P}$ is the factor that describes the increasing of membrane resistance due to the liquid sorption in the polymer. Thus, Eq. (13) states that the overall resistance to gas transfer is the sum of the liquid film resistance and the pure polymer membrane resistance multiplied by sorption (wetted) factor.

The volume fraction of the used RTIL in PTMSP can be estimated from the following relation (assuming volume additivity upon mixing):

$$\phi = \frac{w}{w + (1-w)\,\rho/\rho_{\mathrm{p}}} \tag{14}$$

where w is the weight fraction of RTIL in PTMSP, ρ = 1.28 g/cm^3 and ρ_{p} = 0.78 g/cm^3 are the densities of the [Emim][BF_4] and PTMSP, respectively. Our sorption measurements resulted in w = 2 wt %, so that the volume fraction ϕ = 1.3 vol. %. This value was used for the evaluation of membrane resistance.

The permeability coefficient of CO_2 in used RTIL is also needed for the membrane resistance calculation and can be taken from works considering gas permeability of supported liquid membranes (Jiang et al., 2007; Scovazzo et al., 2009). Despite the use of very similar microporous supports (a hydrophilic polyethersulfone support with 80% porosity), average permeability values obtained in these papers differ for almost 2-fold. Such difference in permeability seems to be related not only to the difference between the measurement techniques but also to the IL purity (moisture content and other impurities). It should be noted that that authors of (Scovazzo et al., 2009) state that their measurements are "the gas permeabilities of free liquid RTIL and not the permeabilities of RTIL-membranes". The data for two published values of permeabilities for [Emim][BF_4] are summarized in the Table 3. Permeability coefficient of pure PTMSP membrane (P_{p}) is much greater than for the ionic liquid (P). However, sorption of

[Emim][BF_4] in the polymer reduces the permeability coefficient of the membrane by 26-42% (P_m), depending on the reference value of the P.

Table 3

P_p, P and P_m are the CO_2 permeability coefficients (in barrer) of pure PTMSP, [Emim][BF_4] and the membrane (membrane thickness is 21 μm), respectively; β is sorption factor at ϕ = 1.3 vol. %, R_m is the membrane resistance (in 1/GPU).

P_p	P	P_m	β	R_m
27600	480 (Jiang et al., 2007)	15912	1.76	$1.34 \cdot 10^{-3}$
	968 (Scovazzo et al., 2009)	20329	1.38	$1.05 \cdot 10^{-3}$

According to our estimates (see Fig. 6), the reciprocal overall MTC (i.e. the overall resistance) is varied from 0.04 to 0.016 GPU^{-1} with the liquid velocity. The membrane resistance (Table 3) is an order of magnitude less than the overall resistance. The fraction of the membrane resistance $R_m/R^{(g)}$ for the two values of CO_2 permeability in the ionic liquid is shown in Fig. 7.

In the case of P = 468 barrer, this contribution ranges from 3.4 to 8.1% as liquid velocity increase from 0.33 to 21 cm/s. If the CO_2 permeability of the ionic liquid is equal to 986 barrer, the largest contribution of the membrane to the overall resistance is 6.3%. In any case, it is evident that the liquid phase mass transfer resistance is the dominating contribution to the overall resistance. As can be seen from Fig. 7, the higher the liquid flow rate, the greater the contribution of the membrane resistance into overall resistance. As the permeability coefficients are independent of the liquid velocity, the second term in Eq. (13) is also independent of the liquid velocity. Then, the sole reason for the increase of the membrane resistance contribution is the liquid phase resistance decrease. This decrease can occur by reducing the thickness of liquid boundary layer.

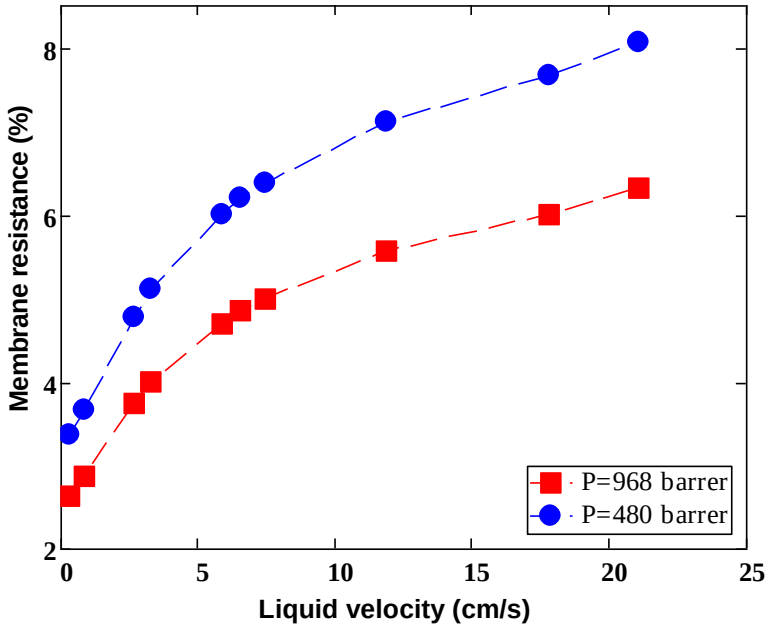

Fig. 7. The membrane contribution to overall mass-transfer resistance at two literature values of the CO_2 permeability of [Emim][BF_4]; volume fraction of [Emim][BF_4] is 1.3 %; thickness of the unswollen membrane is 21 μm; temperature is 30ºC.

The boundary layer thickness can be determined once the overall and membrane resistances are known. It follows from Eq. (13) that

$$\delta = P\left(R^{(g)} - R_{\mathrm{m}}\right) \tag{15}$$

at given liquid velocity. Obtained data has been fitted with the power function

$$\delta^{-1}(u) = au^{q} + b \tag{16}$$

The best fit of this function to the data calculated from Eq. (15) is obtained for the following parameters: $a = 0.022, b = 0.010, q = 0.312$ if CO_2 permeability coefficient in the RTIL $P = 968$ barrer and $a = 0.046, b = 0.019, q = 0.310$ if $P = 480$ barrer (Fig. 8). It should be noted that $\delta^{-1} \square u^{0.31}$ in both cases. As expected, the boundary layer thickness decreases with the liquid velocity. The liquid film thickness velocity is higher in the case of $P = 968$ barrer, than in the case of $P = 480$ barrer.

As known, liquid phase mass transfer coefficient k_{L} in dimensionless form is the Sherwood number. As $k_{\mathrm{L}} = D/\delta$, the Sherwood number is expressed as

$$\mathrm{Sh} \equiv \frac{k_{\mathrm{L}} d_{\mathrm{h}}}{D} = \frac{d_{\mathrm{h}}}{\delta} \tag{17}$$

where d_h is the hydraulic diameter of the channel, D is the gas diffusivity across the liquid boundary layer. In the case of the slit channel $d_h \cong 2h$ with h being the channel height. The value of the liquid film thickness can be predicted from Sherwood relations, which are represented as $\mathrm{Sh} = c\,\mathrm{Re}^q\,\mathrm{Sc}^r$ (Gabelman and Hwang, 1999). Here Re is the Reynolds number ($\mathrm{Re} = \rho u d_h / \mu$), Sc is the Schmidt number ($\mathrm{Sc} = \mu / \rho D$), μ is the liquid viscosity, and c, q, and r are adjustable parameters. These parameters depend on the flow conditions (laminar, turbulent), the membrane module design, etc.

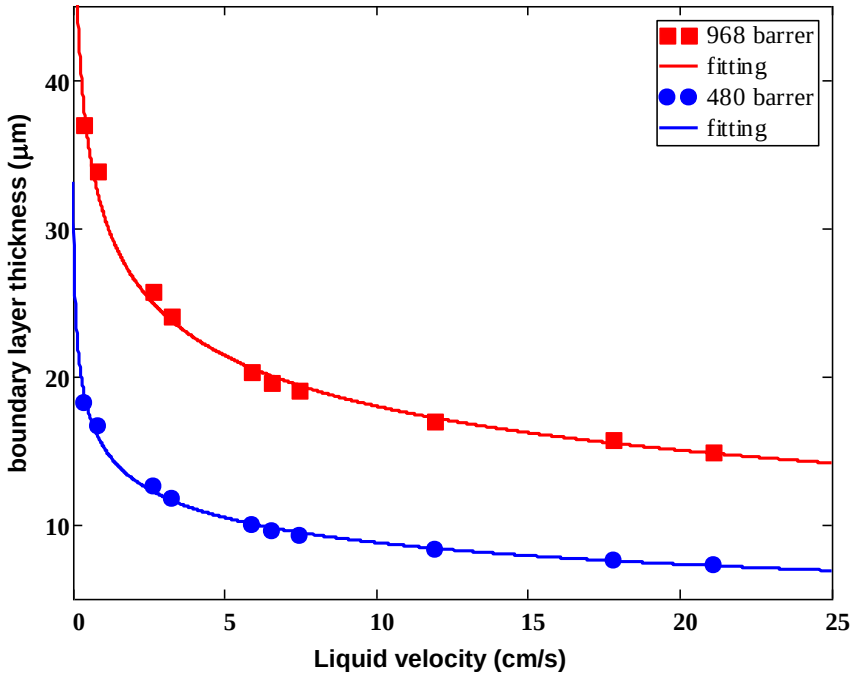

Fig. 8. The thickness of liquid boundary layer as a function of the RTIL velocity at two literature values of CO_2 permeability across [Emim][BF_4]. Points are the calculated values based on experiment and resistance-in-series model (Eq. (15)), solid lines were fitted using the power function of Eq. (16).

For the flow of ionic liquid [Emim][BF_4] in the slit channel, the range of the Reynolds numbers was found to be 0.02-1.4. Sherwood's correlations for so small Reynolds numbers are uncommon in the literature. In this respect, it is necessary to notice the articles of Sirkar and coworkers (Bhaumik et al., 1998; Mulukutla et al., 2014) in which the following correlation was used for hollow fiber membranes:

$$\mathrm{Sh} = 0.57\,\mathrm{Re}^{0.31}\,\mathrm{Sc}^{0.33} \quad \text{for} \quad 0.01 < \mathrm{Re} < 1 \tag{18}$$

In this situation, as follows from Eqs. (17) and (18), the reciprocal thickness of the liquid film is proportional to the liquid velocity with the exponent coefficient 0.31. It is interesting to

note that the same exponent is obtained by us above in the approximation of the boundary layer thickness. Moreover, our data presented in Fig.8 shows quantitative fit with the Eq. (18) at an insignificant correction of the first factor in this equation.

The experiments were carried out for two cases: (1) absorption and stripping temperatures are equal; (2) stripping temperature is higher than the absorption one. The CO_2-saturated RTIL is pressurized up to 10 bar for both cases. The CO_2 stripping flux was measured after achieving steady state. The results are presented in Fig. 9 (for convenience, the flux is also given in units of $kg \cdot m^{-2} \cdot h^{-1}$). As expected, the CO_2 stripping flux increases with application of higher temperatures: temperature rise from 30 to 50°C increases the CO_2 flux by more than 30%. This is the result of lower CO_2 solubility in [Emim][BF_4] (Soriano et al., 2008). Thus the increasing of temperature is a promising operation to enhance the CO_2 stripping process.

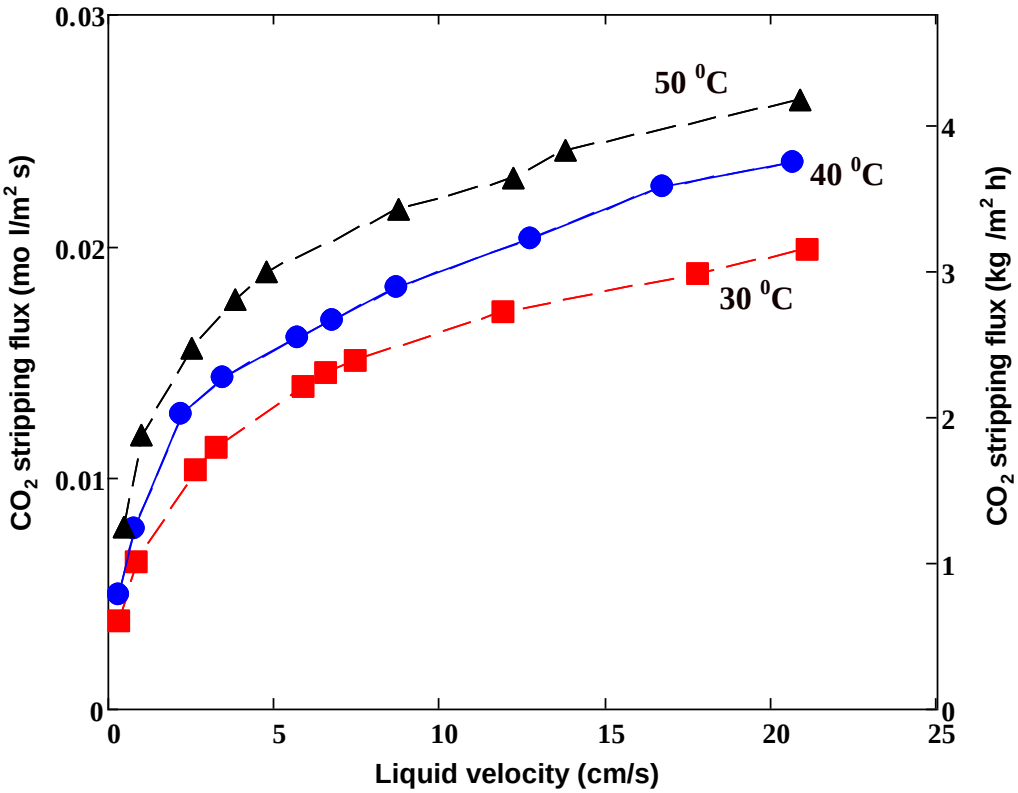

Fig. 9. The stripping CO_2 flux vs. the liquid velocity at different stripping temperatures in the dense membrane contactor.

As shown earlier (Trusov et al., 2011; Bazhenov et al., 2012; Grekhov et al., 2012; Volkov et al., 2013), PTMSP possesses barrier properties towards different solvents at higher temperatures and pressures (up to 100°C and 50 bar). This allows to further intensify CO_2 stripping flux within dense PTMSP membrane contactor.

5. Conclusions

In this study, we provide the proof-of-concept of CO_2 stripping from ionic liquids as a solvent with membrane contactor at elevated trans-membrane pressure. For this purpose, we used dense flat-sheet membranes made from highly permeable polymer PTMSP. To prove the possibility of its application, a screening test on the membrane-RTIL compatibility in nine different ionic liquids was carried out. The results clearly depicted that the interaction of RTILs with PTMSP is correlated with liquid surface tension: the higher the surface tension of RTIL, the lower the values of sorption and volumetric swelling degree. The liquid-polymer interactions were studied by FTIR spectroscopy for RTILs with least ([Emim][DCA], [Emim][BF_4]) and highest ([P66614][Br], [P66614][Phos]) sorption values. It turned out that cations and anions of RTILs can coordinate towards oppositely charged PTMSP atoms thus causing chain conformation change and electron density redistribution within the polymeric unit. FTIR results correspond well to sorption data. Finally, the long-term RTIL permeation study confirmed that PTMSP membranes are indeed impermeable to [Emim][DCA] and [Emim][BF_4] at a trans-membrane pressure of 40 bar, that makes it possible to use these RTILs as CO_2 solvents within membrane contactors.

CO_2 stripping tests were carried out in the flat sheet membrane contactor at temperature 30°C and transmembrane pressure 10 bar using [Emim][BF_4] as a demo solvent. Results indicated that CO_2 stripping flux J increases, and, in contrast, the stripping efficiency η decrease with the liquid flow rate. Under optimal liquid velocity value (when the product of J and η is maximal), J = 1.2 kg/m^2·h and η = 48%. Using the resistance-in-series model, the membrane resistance contribution to the gas transfer was estimated about 8% under the maximum liquid velocity, which means that the main mass transfer resistance is located in the liquid boundary layer. Experiments showed that the increasing of stripping temperature from 30 to 50°C gives the possibility to obtain significant (30% and higher) growth of the CO_2 stripping flux in the membrane contactor. PTMSP membranes provide an absence of solvent leakage at elevated temperatures and pressures. This lays the groundwork for further increasing of CO_2 stripping performance from RTILs using dense ultrapermeable membranes.

Acknowledgements

This work was done as part of TIPS RAS State Plan. Thijs J.H.Vlugt acknowledges NWO-CW for a VICI grant. The authors express their gratitude to J.V. Kostina (TIPS RAS) for the providing FTIR analysis data.

References

Akhmetshina, A.I., Gumerova, O.R., Atlaskin, A.A., Petukhov, A.N., Sazanova, T.S., Yanbikov, N.R., Nyuchev, A.V., Razov, E.N., Vorotyntsev, I.V., 2017. Permeability and selectivity of acid gases in supported conventional and novel imidazolium-based ionic liquid membranes. Sep. Purif. Technol. 176, 92-106.

Albo, J., Luis, P., Irabien, A., 2011. Absorption of coal combustion flue gases in ionic liquids using different membrane contactors. Desalination and Water Treatment 27, 54-59.

Andreeva, L.V., Maksimov, A.L., Zhuchkova, A.Y., Predeina, V.V., Filippova, T.Y., Karakhanov, E.A., 2007. Oxidation of unsaturated compounds in ionic liquids with the use of cyclodextrin-containing catalytic systems. Petrol. Chem. 47, 331-336.

Bazhenov, S., Lysenko, A., Dibrov, G., Vasilevsky, V., Khotimsky, V., Volkov, A., 2012. High Pressure Regeneration of MDEA in Membrane Gas-liquid Contactor. *Procedia Engineering* 44, 1185-1187.

Bazhenov, S., Ramdin, M., Volkov, A., Volkov, V., Vlugt, T.J., de Loos, T.W., 2014. CO_2 Solubility in biodegradable hydroxylammonium-based ionic liquids. J. Chem. Eng. Data 59, 702-708.

Bazhenov, S.D., Lyubimova, E.S., 2016. Gas–liquid membrane contactors for carbon dioxide capture from gaseous streams. Petrol. Chem. 56, 889-914.

Beggel, F., Nowik, I.J., Modigell, M., Shalygin, M.G., Teplyakov, V.V., Zenkevitch, V.B., 2010. A novel gas purification system for biologically produced gases. J. Cleaner Production 18, S43-S50.

Bhaumik, D., Majumdar, S., Sirkar, K.K., 1998. Absorption of CO_2 in a transverse flow hollow fiber membrane module having a few wraps of the fiber mat. J. Membr. Sci. 138, 77–82.

Bitter, J.G.A., 1984. Effect of crystallinity and swelling on the permeability and selectivity of polymer membranes. Desalination 51, 19-35.

Camper, D., Becker, C., Koval, C., Noble, R., 2005. Low pressure hydrocarbon solubility in room temperature ionic liquids containing imidazolium rings interpreted using regular solution theory, Ind. Eng. Chem. Res. 44, 1928-1933.

Chau, J., Obuskovic, G., Jie, X., Sirkar, K.K., 2014. Pressure swing membrane absorption process for shifted syngas separation: modeling vs. experiments for pure ionic liquid. J. Membr. Sci. 453, 61–70.

Cussler, E.L., 1994. Hollow fiber contactors, in: Crespo, J.G., Boddeker, K.W. (Eds.), Membrane Processes in Separation and Purification, Springer, pp. 375-393.

Dai, Z., Deng, L., 2016. Membrane absorption using ionic liquid for pre-combustion CO_2 capture at elevated pressure and temperature. Int. J. Greenhouse Gas Control 54, 59-69.

Dai, Z., Noble, R.D., Gin, D.L., Zhang, X., Deng, L., 2016a. Combination of ionic liquids with membrane technology: A new approach for CO_2 separation. J. Membr. Sci. 497, 1–20.

Dai, Z., Usman, M., Hillestad, M., Deng, L., 2016b. Modelling of a tubular membrane contactor for pre-combustion CO_2 capture using ionic liquids: Influence of the membrane configuration, absorbent properties and operation parameters. Green Energy & Environment 1, 266-275.

Dai, Z., Ansaloni, L., Deng, L., 2016c. Pre-combustion CO_2 Capture in Polymeric Hollow Fiber Membrane Contactors Using Ionic Liquids: Porous Membrane versus Nonporous Composite Membrane. Ind. Eng. Chem. Res. 55, 5983–5992.

Dibrov, G.A., Volkov, V.V., Vasilevsky, V.P., Shutova, A.A., Bazhenov, S.D., Khotimsky, V.S., van de Runstraat, A., Goetheer, E.L.V., Volkov, A.V., 2014. Robust high-permeance PTMSP composite membranes for CO_2 membrane gas desorption at elevated temperatures and pressures. J. Membr. Sci. 470, 439-450.

Dindore, V.Y., Brilman, D.W.F., Geuzebroek, F.H., Versteeg, G.F., 2004. Membrane–solvent selection for CO_2 removal using membrane gas–liquid contactors. Sep. Purif. Technol. 40, 133-145.

Filippov, A.N., Ivanov, V.I., Yushkin, A.A., Volkov, V.V., Bogdanova, Yu.G., Dolzhikova, V.D., 2015. Simulation of the Onset of Flow through a PTMSP-Based Polymer Membrane during Nanofiltration of Water–Methanol Mixture. Petrol. Chem. 55, 247-362.

Gabelman, A., Hwang, S.-T., 1999. Hollow fiber membrane contactors. J. Membr. Sci. 159, 61-106.

Ghadiri, M., Marjani, A., Shirazian, S., 2013. Mathematical modeling and simulation of CO_2 stripping from monoethanolamine solution using nano porous membrane contactors. Int. J. Greenhouse Gas Control 13, 1–8.

Gómez-Coma, L., Garea, A., Irabien, A., 2014. Non-dispersive absorption of CO_2 in [emim][$EtSO_4$] and [emim][Ac]:temperature influence. Sep. Purif. Technol. 132, 120–125.

Gómez-Coma, L., Garea, A., Rouch, J.C., Savart, T., Lahitte, J.F., Remigy, J. C., Irabien, A., 2016. Carbon dioxide capture by [emim][Ac] ionic liquid in a polysulfone hollow fiber membrane contactor. Int. J. Greenhouse Gas Control 52, 401-409.

Grekhov, A., Belogorlov, A., Yushkin, A., Volkov, A., 2012. New express dynamic technique for liquid permeation measurements in a wide range of trans-membrane pressures. J. Membr. Sci. 390-391, 160-163.

Hallett, J.P., Welton, T., 2011. Room-temperature ionic liquids: solvents for synthesis and catalysis. 2. Chem. Rev. 111, 3508-3576.

Ionic Liquids Database - ILThermo (v2.0), Accessed 7 July, 2016. http://ilthermo.boulder.nist.gov (visited in May 2017)

Jain, N., Kumar, A., Chauhan, S., Chauhan, S.M.S., 2005. Chemical and biochemical transformations in ionic liquids. Tetrahedron 61, 1015-1060.

Jiang, Y.-Y., Zhou, Z., Jiao, Z., Li, L., Wu, Y.-T., Zhang, Z.-B., 2007. SO_2 gas separation using supported ionic liquid membranes. J. Phys. Chem. B 111, 5058-5061.

Jie, X.M., Chau, J., Obuskovic, G., Sirkar, K.K., 2013. Preliminary studies of CO_2 removal from pre-combustion syngas through pressure swing membrane absorption process with ionic liquid as absorbent. Ind. Eng. Chem. Res. 52, 8783–8799.

Lei, Z., Dai, C., Chen, B., 2014. Gas solubility in ionic liquids. Chem. Rev. 114, 1289-1326.

Legkov, S.A., Bondarenko, G.N., Kostina, J.V., 2012. Structural features of disubstituted polyacetylenes with bulky substituents at double bonds. Polym. Sci. Ser. *A* 54, 187-194.

Karadas, F., Atilhan, M., Aparicio, S., 2010. Review on the use of ionic liquids (ILs) as alternative fluids for CO_2 capture and natural gas sweetening. Energy Fuels 24, 5817-5828.

Khaisri, S., deMontigny, D., Tontiwachwuthikul, P., Jiraratananon, R., 2011. CO_2 stripping from monoethanolamine using a membrane contactor. J. Membr. Sci. 376, 110–118.

Khotimsky, V.S., Tchirkova, M.V., Litvinova, E.G., Rebrov, A.I., Bondarenko, G.N., 2003. Poly[1-trimethylgermyl)-1-propyne] and poly[1-(trimethylsilyl)-1-propyne] with various geometries: their synthesis and properties. J. Polym. Sci., Part A 41, 2133-2155.

Lu, J. G., Lu, C. T., Chen, Y., Gao, L., Zhao, X., Zhang, H., Xu, Z. W., 2014. CO_2 capture by membrane absorption coupling process: application of ionic liquids. Applied Energy, 115, 573-581.

MacFarlane, D.R., Forsyth, M., Howlett, P.C., Pringle, J.M., Sun, J., Annat, G., Neil, W., Izgorodina, E., 2007. Ionic liquids in electrochemical devices and processes: Managing interfacial electrochemistry. Acc. Chem. Res. 40, 1165−1173.

Mansourizadeh, A., Ismail, A.F., 2011. CO_2 stripping from water through porous PVDF hollow fiber membrane contactor, Desalination 273, 386–390.

Mosadegh-Sedghi, S., Rodrigue, D., Brisson, J., Iliuta, M.C., 2014. Wetting phenomenon in membrane contactors – Causes and prevention. J. Membr. Sci. 452, 332-353.

Mulukutla, T., Obuskovic, G., Sirkar, K.K., 2014. Novel scrubbing system for post-combustion CO_2 capture and recovery: Experimental studies. J. Membr. Sci. 471, 16–26.

Nguyen, P.T., Lasseuguette, E., Medina-Gonzalez, Y., Remigy, J.C., Roizard, D., Favre, E., 2011. A dense membrane contactor for intensified CO_2 gas/liquid absorption in post-combustion capture. J. Membr. Sci. 377, 261– 272.

Rahbari-Sisakht, M., Ismail, A.F., Rana, D., Matsuura, T., 2013a. Carbon dioxide stripping from diethanolamine solution through porous surface modified PVDF hollow fiber membrane contactor. J. Membr. Sci. 427, 270–275.

Rahbari-Sisakht, M., Ismail, A.F., Rana, D., Matsuura, T., Emadzadeh, D., 2013b. Carbon dioxide stripping from water through porous polysulfone hollow fiber membrane contactor. Sep. Purif. Tech. 108, 119–123.

Ramdin, M., de Loos, T.W., Vlugt, T.J.H., 2012. State-of-the-art of CO_2 capture with ionic liquids. Ind. Eng. Chem. Res. 51, 8149−8177.

Ramdin, M., Amplianitis, A., Bazhenov, S., Volkov, A., Volkov, V., Vlugt, T.J.H., de Loos, T.W., 2014. Solubility of CO_2 and CH_4 in ionic liquids: ideal CO_2/CH_4 selectivity. Ind. Eng. Chem. Res. 53, 15427-15435.

Robeson, L.M., 2010. Polymer blends in membrane transport processes, Ind. Eng. Chem. Res. 49, 11859–11865.

Scholes, C.A., Kentish, S.E., Stevens, G.W., Jin, J., deMontigny, D., 2015. Thin-film composite membrane contactors for desorption of CO_2 from Monoethanolamine at elevated temperatures. Sep. Purif. Tech. 156, 841–847.

Scholes, C.A., Qader, A., Stevens, G.W., Kentish, S.E., 2014. Membrane gas-solvent contactor pilot plant trials of CO_2 absorption from flue gas. Sep. Sci. Technol. 49, 2449–2458.

Scovazzo, P., Havard, D., McShea, M., Mixon, S., Morgan, D., 2009. Long-term, continuous mixed-gas dry fed CO_2/CH_4 and CO_2/N_2 separation performance and selectivities for room temperature ionic liquid membranes. J. Membr. Sci. 327, 41–48.

Shalygin, M.G., Roizard, D., Favre, E., Teplyakov, V.V., 2008. CO_2 transfer in an aqueous potassium carbonate liquid membrane module with dense polymeric supporting layers: Influence of concentration, circulation flow rate and temperature. J. Membr. Sci. 318, 317-326.

Shutova, A.A., Trusov, A.N., Bermeshev, M.V., Legkov, S.A., Gringolts, M.L., Finkelstein, E.Sh., Bondarenko, G.N., Volkov, A.V., 2014. Regeneration of alkanolamine solutions in membrane contactor based on novel polynorbornene. Oil & Gas Science and Technology 69, 1059-1069.

Sirkar, K.K., 1992. Other new membrane processes, in: Ho, W.S.W., Sirkar, K.K. (Eds.), Membrane Handbook, Chapman and Hall, New York, pp. 885-912.

Soriano, A.N., Doma Jr., B.T., Li, M.H., 2008. Solubility of carbon dioxide in 1-ethyl-3-methylimidazolium tetrafluoroborate. J. Chem. Eng. Data 53, 2550-2555.

Sun, P., Armstrong, D.W., 2010. Ionic liquids in analytical chemistry. Analytica Chimica Acta 661, 1-16.

Trusov, A., Legkov, S., van den Broeke, L.J.P., Goetheer, E., Khotimsky, V., Volkov, A., 2011. Gas/liquid membrane contactors based on disubstituted polyacetylene for CO_2 absorption liquid regeneration at high pressure and temperature. J. Membr. Sci. 383, 241-249.

Vlugt, T.J.H., Volkov, A., 2015. Study of glassy polymers fractional accessible volume (FAV) by extended method of hydrostatic weighing: Effect of porous structure on liquid transport. Reactive & Functional Polymers 86, 269-281.

Volkov, A.V., Fedorov, E.V., Malakhov, A.O., Volkov, V.V., 2002. Vapor sorption and dilation of poly[(1-trimethylsilyl)-1-propyne] in methanol, ethanol and propanol. Polym. Sci. Ser. B 44, 158-162.

Volkov, A., Yushkin, A., Grekhov, A., Shutova, A., Bazhenov, S., Tsarkov, S., Khotimsky, V., Vlugt, T.J.H., Volkov, V., 2013. Liquid permeation through PTMSP: One polymer for two different membrane applications. J. Membr. Sci. 440, 98-107.

Volkov, A.V., Tsarkov, S.E., Goetheer, E.L.V., Volkov, V.V., 2015. Amine-based solvents regeneration in gas-liquid membrane contactor based on asymmetric PVTMS. Petrol. Chem. 55, 716-723.

Yushkin A., Grekhov A., Matson S., Bermeshev M., Khotimsky V., Finkelstein E., Budd P.M., Volkov V., Vlugt T.J.H., Volkov A., 2015. Study of glassy polymers fractional accessible volume (FAV) by extended method of hydrostatic weighing: Effect of porous structure on liquid transport. Reactive and Functional Polymers. 86, 269-281.

Zhao, S., Feron, P.H., Deng, L., Favre, E., Chabanon, E., Yan, S., Hou, J., Chen, V., Qi, H., 2016. Status and progress of membrane contactors in post-combustion carbon capture: A state-of-the-art review of new developments. J. Membr. Sci. 511, 180-206.

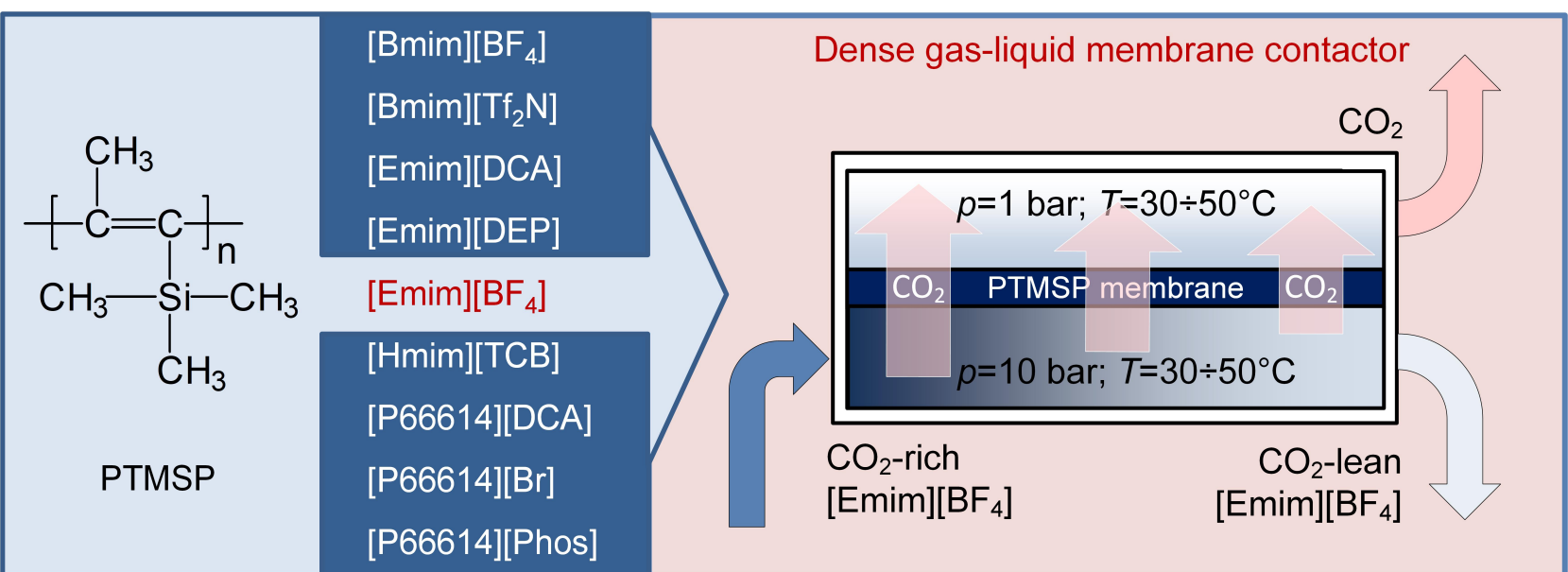
PTMSP
[Bmim][BF4]
[Bmim][Tf2N]
[Emim][DCA]
[Emim][DEP]
[Emim][BF4]
[Hmim][TCB]
[P66614][DCA]
[P66614][Br]
[P66614][Phos]
Dense gas-liquid membrane contactor
CO2
p=1 bar; T=30÷50°C
CO2
PTMSP membrane
CO2
p=10 bar; T=30÷50°C
CO2-rich
[Emim][BF4]
CO2-lean
[Emim][BF4]